



HAL
open science

Channel widening downstream of valley gorges influenced by flood frequency and floodplain roughness

Thomas Croissant, Dimitri Lague, Philippe Davy

► **To cite this version:**

Thomas Croissant, Dimitri Lague, Philippe Davy. Channel widening downstream of valley gorges influenced by flood frequency and floodplain roughness. *Journal of Geophysical Research: Earth Surface*, 2019, 124 (1), pp.154-174. 10.1029/2018JF004767 . insu-01963021

HAL Id: insu-01963021

<https://insu.hal.science/insu-01963021>

Submitted on 25 Jan 2019

HAL is a multi-disciplinary open access archive for the deposit and dissemination of scientific research documents, whether they are published or not. The documents may come from teaching and research institutions in France or abroad, or from public or private research centers.

L'archive ouverte pluridisciplinaire **HAL**, est destinée au dépôt et à la diffusion de documents scientifiques de niveau recherche, publiés ou non, émanant des établissements d'enseignement et de recherche français ou étrangers, des laboratoires publics ou privés.

RESEARCH ARTICLE

10.1029/2018JF004767

Key Points:

- Flood frequency and valley confinement have a dominant effect on long-term bedload transport capacity
- Floodplain vegetation only increases long-term bedload transport capacity for variable climate regimes
- Braided river regime is a means to maintain long-term transport capacity at bedrock gorge/alluvial plain transition

Supporting Information:

- Supporting Information S1

Correspondence to:

T. Croissant,
thomas.croissant@durham.ac.uk

Citation:

Croissant, T., Lague, D., & Davy, P. (2019). Channel widening downstream of valley gorges influenced by flood frequency and floodplain roughness. *Journal of Geophysical Research: Earth Surface*, 124. <https://doi.org/10.1029/2018JF004767>

Received 22 MAY 2018

Accepted 13 DEC 2018

Accepted article online 18 DEC 2018

Channel Widening Downstream of Valley Gorges Influenced by Flood Frequency and Floodplain Roughness

Thomas Croissant¹ , Dimitri Lague¹ , and Philippe Davy¹ 

¹Géosciences Rennes, OSUR, CNRS, Université de Rennes 1, Campus de Beaulieu, Rennes, France

Abstract Mountain fronts are the locus of significant variations in river width characterized by narrow bedrock gorges opening to wider unconfined alluvial rivers that are often braided. The contribution of the abrupt change in river valley confinement in modulating the long-term transport capacity and the resulting equilibrium channel width has never been considered. Here we use a numerical model integrating the full frequency-magnitude distribution of streamflow to explore the long-term bedload transport capacity of idealized confined and unconfined channels, both single thread and braided. The model predicts a significant transport capacity loss for a single channel of constant width at the transition between confined gorges and unconfined floodplains that is slightly reduced when floodplain vegetation is present. Because the total transport capacity of a single-thread channel systematically decreases with channel width in a stochastic framework, only narrower unconfined channels could compensate for the loss of confinement. This prediction contradicts observations of widening ratios ranging from three to eight downstream of gorges in various world rivers. We resolve this inconsistency by demonstrating that a braided river made of narrow channels inset in a wide floodplain can maintain the total bedload transport capacity downstream of gorges by increasing the range of competent discharges. We also show that riparian vegetation may only enhance bedload transport capacity for highly variable discharge regimes and discuss the relevance of various definitions of representative discharges. These results point to the previously unrecognized role of valley confinement in modulating the sediment transport capacity of rivers.

1. Introduction

Mountainous areas systematically exhibit major changes in river confinement that are characterized by width variations between narrow bedrock gorges and wider unconfined alluvial sections. For instance, the ratio between the width of the unconfined and confined channel sections can be as high as a factor 5 in the Rakaia and the Waiau rivers in New Zealand (Figure 1). In many cases, the loss of confinement also corresponds to a transition from a single-thread gorge to an unconfined braided river, a result that is consistent with recent flume experiments (Garcia Lugo et al., 2015). Channel narrowing and gorge development are generally interpreted as a morphologic response to accommodate bedrock incision in response to localized tectonic uplift (e.g., Lavé & Avouac, 2001; Turowski et al., 2009; Yanites & Tucker, 2010) or changes in the mechanical resistance of channel banks (Finnegan et al., 2005). However, a unifying theory explaining river narrowing in response to tectonic uplift under various conditions is still missing (Lague, 2014).

Downstream changes in channel width, which may or may not be associated with channel slope variations, will modify flow depth for a given discharge, in turn changing bed shear stress and the capacity to transport bedload sediment and incise bedrock (e.g., Lague, 2010). Valley confinement controls the so-called at-a-station channel geometry, which determines how water flow spreads laterally as discharge increases (Turowski, Hovius, Meng-Long, et al., 2008; Turowski, Hovius, Wilson, et al., 2008). Any longitudinal variation in confinement can therefore alter the capacity to transport sediment during very large events. How confinement variation translates into long-term variations in river transport capacity and equilibrium geometry remains largely unknown and is the main question addressed in this work.

For unconfined channels, the riparian vegetation populating floodplains also plays a role in controlling water depth and flow velocity patterns during overbank discharge events. The impact of floodplain vegetation on flow hydraulics has been extensively studied to improve river management of flood hazards (Bren, 1993; Chow, 1959; Darby, 1999; Hunter et al., 2007; Mason et al., 2003; Rudorff et al., 2014; Tabacchi



Figure 1. Google Earth snapshots of rivers experiencing longitudinal variation in valley confinement and width. (a) Rakaia River, South Island, New Zealand. (b) Waiau River, South Island, New Zealand.

et al., 2000), but its control on sediment transport has received little attention. Previous studies have focused mainly on floodplain sedimentation at flood or yearly timescales (e.g., Camporeale et al., 2013; Tsujimoto, 1999; Vargas-Luna et al., 2015). The role of floodplain vegetation in modulating total channel transport capacity over short and longer timescales (i.e., greater than 10^2 years) has not been explored. Yet this is a prerequisite to understanding how sensitive river sediment transfers are to floodplains vegetation and to evaluating whether numerical models of long-term river dynamics should encompass this climate dependent effect.

Quantifying long-term sediment transport must take into account the wide range of discharges that carry sediment, with the frequency-magnitude discharge distribution that depends on climate (Tucker & Bras, 2000; Wolman & Miller, 1960). This can be accounted for by explicitly integrating sediment transport events over the total range of discharges weighted by their frequency of occurrence. This stochastic description is essential to capture the nonlinearity generated by transport thresholds (Lague, 2014; Molnar et al., 2006; Tucker & Bras, 2000) and to evaluate the role of climate-driven discharge variability that the traditional effective discharge approach (Wolman & Miller, 1960) cannot easily account for (Lague et al., 2005; Tucker & Bras, 2000). Here, following previous work on bedrock river incision (DiBiase & Whipple, 2011; Lague et al., 2005; Molnar et al., 2006; Tucker, 2004), we explore the sensitivity of vegetated alluvial rivers to streamflow variability.

The main aims of this work are to evaluate the impact of confinement and vegetation on long-term transport capacity across the complete spectrum of mean daily discharge. This is evaluated for different discharge variability regimes modulating the occurrence of large discharge events with respect to mean discharge. We investigate how channel geometry varies at the transition between bedrock gorges and alluvial plains and how it could be related to change in valley confinement. We also aim at discussing the degree of underestimation of long-term bedload transport capacity occurring when a unique representative discharge is used rather than the complete spectrum of daily stream flow and whether the notion that bankfull discharge is the effective discharge (Andrews, 1980; Simon et al., 2004) is valid for different confinement, vegetation, and climate scenarios.

More specifically, we address the following:

1. Does the change in confinement between bedrock and alluvial rivers, modulated by vegetation, significantly alter the long-term transport capacity and can it explain the systematic widening observed at confined/unconfined transitions?
2. Is there a causal link between the braiding instability and the loss of confinement upstream and downstream of gorges?

3. Does discharge variability and the variable friction introduced by vegetation need to be accounted for when predicting sediment transport capacity of rivers over longer than secular timescales, with relevance for the morphodynamics of river and landscape evolution in the context of climate change?
4. To what extent is the long-term transport capacity underestimated when using an effective discharge (as opposed to the entire hydrograph) and how are the results influenced by discharge variability and riparian vegetation?

We start by presenting the simplified hydraulic model developed for this study and the computation of long-term bedload and suspended load transport capacity over a range of daily stream flows covering several orders of magnitude. We systematically study the influence of confinement, discharge variability, and floodplain roughness on long-term transport capacity for spatially uniform conditions and revisit the relationship between representative discharge and long-term transport capacity as a function of discharge variability. Finally, we explore the response of rivers at the confined/unconfined transition of bedrock gorges in terms of channel width and channel type (single channel vs. braided systems).

2. Methods

In the following, we start by presenting the theoretical background used to develop the analytical approach. We first describe the simplified cross-section geometries that we have used to model confined gorges, unconfined single-thread channels, and braided rivers. Then we present how long-term sediment transport capacity is calculated, using elementary transport laws that are integrated over the full magnitude-frequency distribution of daily streamflow. The various definitions of representative discharges used in previous studies are summarized, followed by the methods used to estimate widening factors downstream of bedrock gorges in natural cases.

2.1. Channel Cross-Section Geometries

The transport capacity laws used in this study are dependent on the scaling relationship between shear stress and water discharge, which is controlled by the river hydraulic geometry. In the following, we describe the different channel cross-section geometries for single-thread and braided rivers that are two end-members of unconfined river systems (Figure 2).

2.1.1. Unconfined Single-Thread Channel

The unconfined single-thread channel cross section is represented by a rectangular channel set into a wide floodplain with bankfull width W_{ch} , channel slope S , and bankfull depth dh (Figure 2b). To define a representative channel geometry, we use the semiempirical relationship derived by Parker et al. (2007) from a large data set of gravel bed rivers. In this model, W_{ch} , S , and dh depend only on bankfull discharge Q_{bf} and median grain size D_{50} of channel bed material. We set our study in the context of gravel bed rivers and arbitrarily choose $D_{50} = 0.05$ m, defined as coarse gravel in the Wentworth scale. We set $Q_{bf} = 500$ m³/s such that $W_{ch} = 82$ m, $S = 0.0013$, and $dh = 2.9$ m. This represents an average geometry in the data set used by Parker et al. (2007). The floodplain width, W_{fp} , is set arbitrarily to 200 m. The relevance of our findings for other floodplain widths is addressed in the discussion section. A Manning friction coefficient of 0.04, which is typical of natural gravel bed streams, is used for the channel. Friction coefficients from 0.04 to 0.15 are assigned to the floodplain depending on vegetation height and density according to Manning coefficients derived from previous studies (Table 1; Arcement & Schneider, 1989; Casas et al., 2010; Chow, 1959; Cobby et al., 2003; Mason et al., 2003; Powell, 2014; Rudorff et al., 2014; Werner et al., 2005). To assess the effect of floodplain vegetation on sediment transport capacity for different water stages within the channel, we explore a range of daily discharges experienced by the river. The choice of the range and the maximum value are justified in section 2.2.3.

To determine the stage-discharge rating curve for overbank discharges, we decompose the cross section in two subsections, the main channel, and the floodplain. Following the “Divided Channel Method” (Bousmar & Zech, 1999; Chow, 1959; Fernandes et al., 2012), the total discharge is described as

$$Q_{total} = Q_{channel} + 2Q_{floodplain}. \quad (1)$$

The discharge for each subsection can be estimated from the Manning resistance equation, assuming a rectangular cross section, a steady uniform flow, and neglecting bank friction:

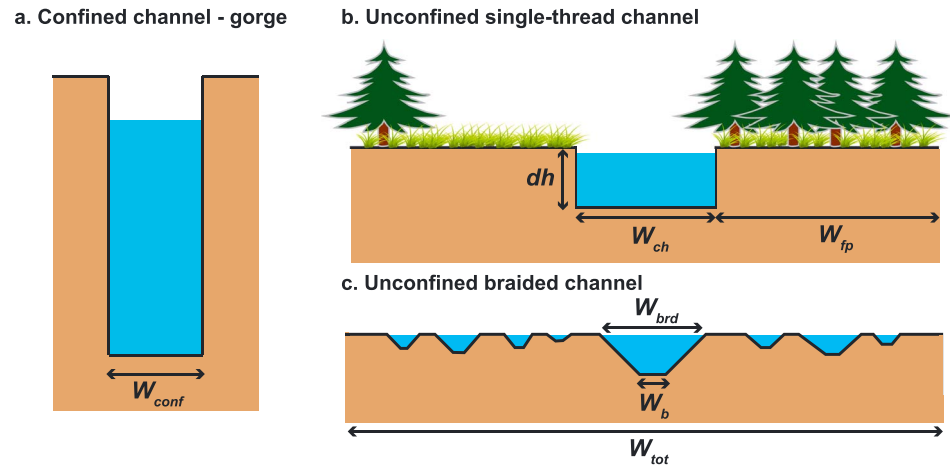


Figure 2. The different channel cross-section geometries used in this study. (a) The confined channel or gorge. (b) The unconfined single-thread channel has a rectangular cross section, and its floodplain can be populated by different vegetation types whose effect on hydraulics is captured by varying the Manning friction coefficient (n_{fp}). For example, on the left bank, dense brush with some sparse trees ($n_{fp} = 0.10$) and on the right bank, dense brush and dense population of trees ($n_{fp} = 0.15$). Notation: W_{ch} = channel width; W_{fp} = floodplain width; dh = bank height. (c) The unconfined braided channel geometry is composed of trapezoidal threads of different sizes. Note that all schematic representations are vertically exaggerated. Notation: W_{brd} = braid surface width; W_b = braid basal width; W_{tot} = total width of the braided plain.

$$Q_{total} = \frac{W_{ch}}{n_{ch}} h_{ch}^{5/3} S^{1/2} + 2 \frac{W_{fp}}{n_{fp}} h_{fp}^{5/3} S^{1/2}, \quad (2)$$

where h is the water depth and n the Manning friction coefficient. Subscripts ch and fp indicate the main channel and floodplain, respectively. By replacing h_{fp} with $h_{ch} + dh$ in the previous equation, values of h_{ch} for the range of discharges are computed with a Newton-Raphson method to obtain channel and floodplain rating curves. Calculations are made with a 10^{-5} m precision in order to obtain distinct h_{ch} values for close discharges. We neglect any potential dependency of the friction coefficient with water depth (Ferguson, 2010) as most of the change in n occurs over low to medium river discharges, that is, events with nil to very low transport capacity for coarse gravel bed rivers.

In the following sections, results are compared with a confined channel of width W_{conf} and infinitely high banks (Figure 2a). This represents an archetype of a rectangular incised bedrock gorge. The width/water depth ratio is always above 10 for the considered discharge range so that the lateral friction can be neglected in the subsequent bed shear stress calculation.

2.1.2. Unconfined Braided Channels

The synthetic reproduction of the complexity of a braid-plain cross section is challenging. Past attempts to model analytically the transport capacity of braided rivers cross sections have relied on a stochastic description of the shear stress distribution in threads (Bertoldi et al., 2009; Nicholas, 2000; Paola, 1996) or by the definition of a morphological indicator derived from the bed elevation frequency distribution (Redolfi et al., 2016). Here we introduce a simplified cross-section geometry composed of several trapezoidal threads (Figure 2c). The geometry of a braided system is described by the total number of threads (N_{thread}), their individual width (W_{brd}), their depth with respect to the braid plain (dh), and the cumulative width of the interbraid bars. The total braided river cross section is created by choosing N_{thread} and by randomly generating the thread width of each braid. The thread depth is defined by an empirical power law relationship linking the braid width and depth ($dh \propto W_{brd}^{0.75}$; Ashmore, 2013).

We assume that the braid plain is at constant elevation (Figure 2c) but that the threads have variable depth, corresponding to different inundation levels. The water increases incrementally from the deepest braid to the surface with smaller braids being activated as the water reaches their

Table 1
Manning Coefficient Values and Examples of Associated Vegetation Type (Powell, 2014)

Manning coefficient value, n_{fp}	Vegetation type
0.04	Gravel, grass, or crops
0.06	Light brush and trees
0.10	Medium to dense brush
0.15	Dense brush and trees

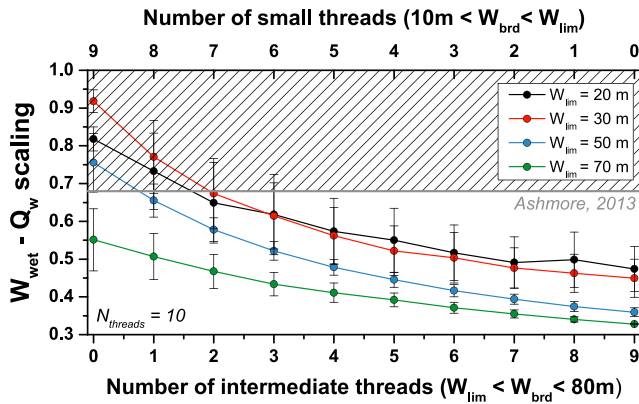


Figure 3. The scaling exponent between the wetted width and discharge for different braid plain configurations. The braid plain is composed of 10 threads classified as main, intermediate, and small. The shaded area corresponds to the range of exponents estimated for natural cases (Ashmore, 2013). Notation: $N_{threads}$ = number of threads; W_{lim} = the width that sets the range of intermediate or small threads.

empirical criteria. The first criterion is an efficient primary filter of the geometries, as the range of parameters that satisfy it is very narrow (Figure 3). We then use the other two criteria to identify successful geometries. Based on the results of our parameter exploration, N_{thread} is fixed at 10 with braid widths ranging from 10 to 100 m (Figures 3 and S3 in the supporting information). We found that our geometries are able to reproduce the above relationships if we use one to three intermediate threads varying between 30 and 80 m and eight to six smaller threads with widths inferior to 30 m.

Natural braided river reaches are often composed of one to two larger channels accompanied by several smaller threads that are successively activated as the river stage increases (Figure 1). In our example, the main channel width is set to 100 m, and the other nine channels widths are randomly generated: Two intermediate threads present a width between 30 and 80 m and seven small threads with a width between 10 and 30 m. Note that using rectangular channels of identical width and depth is too simplistic, as it fails to reproduce observed empirical relationships such as the power law relationship between wetted width and discharge.

2.2. Long-Term Sediment Transport Capacity Calculation

2.2.1. Elementary Transport Laws

We use classic sediment transport laws that express the sediment transport capacity as a function of the shear stress exerted by the flow on the river bed. Shear stress is calculated as

$$\tau = \rho ghS, \quad (3)$$

where ρ is the water density and g the gravitational constant. The transport capacity for bedload material is calculated with the Meyer-Peter and Müller (1948), MPM, law:

$$q_{s,bl} = k_p(\tau - \tau_c)^{1.5}, \quad (4)$$

where k_p is a constant depending on sediment and water density and the gravitational constant and τ_c is the critical shear stress defined as the shear stress necessary to entrain material into bedload. τ_c is calculated assuming a critical Shields number $\tau_c^* \sim 0.03$ ($\tau_c^* = \tau_c / (\rho_s - \rho)gD_{50}$). While the predicted bedload transport capacity will vary with the chosen bedload transport law, our results on the sensitivity to vegetation, discharge variability, and confinement are independent of the specific law used as long as it incorporates a threshold of transport and an asymptotic scaling as $\tau^{1.5}$.

In natural and experimental alluvial channels, bedload transport typically starts when discharge is between 50% and 100% of the bankfull discharge (Mueller et al., 2005; Parker et al., 2007; Pitlick & Cress, 2002; Ryan et al., 2002; Ryan & Emmett, 2002; Talling, 2000). In the following section, the threshold of sediment motion

level. The basal width of a single braid is arbitrarily set to be 10% of W_{brd} to ensure a low bank angle (less than 5°) and because the scaling between total wetted width and discharge is too low for lower values. The relationship between water depth and river discharge, which is critical for the transport capacity calculation, is back-calculated by predicting water depth for increasingly small increments of discharge using the Manning friction law.

To evaluate whether our simplified model generates realistic geometries and hydraulic behavior, we require that three empirical relationships must be fulfilled: (1) The total wetted width should increase as a power law with river discharge, with a power exponent between 0.7 to 1.0 (Ashmore, 2013; Ashmore & Sauks, 2006); (2) the distribution of water depth at bankfull discharge should follow a gamma probability density function (Bertoldi et al., 2009; Nicholas, 2000; Paola, 1996); and (3) the mean water depth should increase more slowly with discharge than the wetted width (Ashmore, 2013).

We have explored the effect of N_{thread} and different channel width distributions to evaluate how these different geometries adhere to these three

is computed to keep $\tau_{bf}/\tau_c = 1.2$ as in (Paola, 1996) and where τ_{bf} is the bankfull bed shear stress of the single-thread channel or of the deepest channel in the braided case. The transport capacity is computed when the shear stress is higher than the threshold of sediment motion in the main channel of the single-thread case and everywhere in the multithread case.

The suspended load transport capacity is determined with the Engelund and Hansen (1967), EH, law:

$$q_{s,susp} = k_{eh}\tau^{2.5}, \quad (5)$$

where k_{eh} is a constant that depends on grain size, sediment density, the gravitational constant, and a friction factor. Although this formula was designed to calculate total load capacity for sand bed rivers, we use it to predict suspended load rates assuming a uniform grain size of fine sediment (0.25 mm). Consequently, we compute the suspended load transport capacity only for discharges that ensure this transport mode (Rouse number less than 2.5).

Our study focuses mainly on bedload transport, because the coarser sediments define the geometry of gravel bed rivers and, thus, control their long-term transport capacity. However, we also consider the predictions for suspended load for two reasons: First, in many rivers, the bulk of the sediment flux is expected to be transported in suspension; second, the EH law offers a contrasting functional relationship with respect to MPM: Both are characterized by a nonlinear relationship between transport capacity (q_s) and river discharge (q), but the MPM nonlinearity emerges from a threshold, while the EH nonlinearity comes from a power law behavior ($q_s \sim q^{1.5}$). This comparison helps in pinpointing fundamental differences in the sensitivity to flood frequency, vegetation, and confinement of bedload and suspended load transport capacity.

2.2.2. Probability Distribution of Daily Discharge

It has been observed that for different worldwide river systems, the complete range of mean daily streamflow can be approximated by an inverse gamma probability density function (Crave & Davy, 2001; DiBiase & Whipple, 2011; Lague, 2014; Lague et al., 2005; Molnar et al., 2006) of the form

$$pdf(Q_m, k) = \frac{k^{k+1}}{\Gamma(k+1)} \exp\left(-\frac{k}{Q^*}\right) Q^{*-(2+k)}, \quad (6)$$

where Q^* is the daily discharge normalized by mean daily discharge Q_m ($Q^* = Q/Q_m$), Γ the gamma function, and k a parameter that controls the shape of the probability density function and captures the variability of the hydrological forcing. The inverse gamma distribution exhibits an exponential tail toward low discharges and a power law tail for large discharges.

To assess the impact of discharge variability, different values of k are used from 0.2 (high variability) to 4 (low variability), consistent with the range of values that have been measured on monitored watersheds (see Figure S1). Note that $k = 4$ represents an extremely low variability regime for which the tail of the probability density function (pdf) can be considered as light, in a sense that large events are extremely rare (Lague, 2014). Values ranging from 0.2 to 1.0 represent highly variable climate conditions typical of monsoon-dominated areas such as Taiwan, which is frequently affected by typhoons (Lague et al., 2005), or arid areas in the United States with infrequent large storms events (Molnar et al., 2006). Deal et al. (2018) and Rossi et al. (2016) have shown that the power law tail of daily streamflow pdf may not be as common as previously thought, at least in the continental United States. We acknowledge the potential limitations of equation (6) but consider it general enough to explore the sensitivity of sediment transport to the mean and variability of daily streamflow.

For an inverse gamma pdf, the return time of a specific daily discharge, Q_{sp} , is given by

$$t_r(Q_{sp}) = \Gamma(k/Q_{sp}, k+1)^{-1}, \quad (7)$$

for any combination of k and Q_m (Lague et al., 2005).

In our approach, the river geometry (W_{ch} , S , and dh) is set by the bankfull discharge of the single-thread channel, but the computation of long-term sediment transport capacity requires characteristics of the discharge distribution (Q_m and k in equation (6)). There is currently no simple theory or model that can link Q_{bf} and Q_m (Phillips & Jerolmack, 2016). Published data sets of single-thread gravel bed rivers shows that

Q_{bf}/Q_m varies between 1.5 and 12, but the sensitivity to discharge variability was not explored in those studies (Andrews, 1980; Andrews & Nankervis, 1995; Pitlick & Cress, 2002; Williams, 1978). It is also commonly observed that the bankfull discharge recurrence time is about 1.5 to 2 years for rivers located in a temperate climate ($k > 2$) and low relief areas (Leopold et al., 1964; Petit & Pauquet, 1997). Based on the previous observation, we set $Q_{bf}/Q_m \sim 5$ for $k = 2$, as it represents the average value of the available data (see Figure S2 for a sensitivity analysis on the impact of Q_{bf}/Q_m on the hydraulic regime and the long-term transport capacity prediction). Under those conditions, the bankfull discharge for an hypothetical case of a river presenting a value of k between 0.2 and 1 has a recurrence interval of ~ 2 months, meaning that competent discharges last several days per year.

2.2.3. Calculation of Long-Term Sediment Transport Capacity

The sediment transport capacity is calculated for each discharge within the total range using equations (4) and (5). Material composing the floodplain usually differs from the main channel bed in terms of grain size and vegetation. As the flow inundates the floodplain, the partitioning between form drag and skin friction changes. A part of the flow energy that contributed to sediment transport is lost because of the supplementary form friction introduced by the fixed roughness elements on the floodplain (e.g., trees and large bushes). As a consequence, the fraction of the shear stress contributing to transport is reduced as the proportion of material causing form friction increases. In addition, the bedload transport model used in this study ignores stress partitioning and bar-form drag in the main channels. For these reasons, floodplains are considered as sediment storage areas so the total sediment transport capacity is computed solely in the main channel in single-thread channels. For braided rivers, transport is also computed on the braid plain, which is typically flooded more often than the floodplain of single-thread channels.

Long-term sediment transport capacity \overline{Q}_s is obtained by integrating the product of event-based sediment transport capacity and its probability of occurrence over the discharge range (Tucker & Bras, 2000):

$$\overline{Q}_s = \int_{Q_c}^{Q_{max}} W_{ch} q_s pdf(Q) dQ, \quad (8)$$

with Q_c defined as the critical discharge able to initiate transport and Q_{max} the maximum discharge experienced by the river during the chosen interval. In doing so we assume that channel geometry (width, longitudinal slope, and bank height), median grain size, and parameters of the frequency-magnitude distribution remain stationary during the timescale of integration. This timescale is a function of the recurrence time of Q_{max} and so depends on climate variability. Considering any k values, the recurrence time of Q_{max} is always under 100 years for equation (8) to converge, that is, for the value of \overline{Q}_s to be independent of Q_{max} . It is thus reasonable to assume that the channel geometry remains approximately steady at the integration timescale if boundary conditions are fixed (mean discharge, grain size, vegetation type, and base level). Predictions for timescales longer than 100–1,000 years with nonstationary boundary conditions are not possible with our approach, as the river geometry may change and a full morphodynamic model should be used.

2.3. Representative Discharge for Single-Thread Channels

In river restoration/engineering as well as in landscape evolution modeling, the action of the complete range of discharges experienced by a river is often reduced to one discharge for convenience and simplicity of computation. This representative discharge, hereafter called Q_{rep} , has been computed or estimated using several approaches that are summarized below.

1. The seminal work of Wolman and Miller (1960) introduced the concept of effective discharge, Q_{eff} , calculated as the discharge that does the most geomorphic work over time. It is defined as the discharge corresponding to the maximum of the product of the discharge probability of occurrence (equation (6)) and event-based transport capacity (equation (4)) over the discharge range (Wolman & Miller, 1960)

$$Q_{eff} = \max(W_{ch} q_s pdf(Q)). \quad (9)$$

Discharge variability is known to affect the effective discharge value by shifting it to higher discharge values as variability increases (i.e., large daily discharge events are more frequent) (Andrews, 1980; Pickup & Warner, 1976; Wolman & Miller, 1960). The effective discharge value is also sensitive to both the exponent of the transport equation and the shape of the pdf used to represent the discharge series (e.g., Barry et al., 2008).

2. The bankfull discharge Q_{bf} is commonly assumed to be the representative discharge given its morphologic signature. Indeed, in the case of gravel bed rivers, several studies have shown that $Q_{eff} \sim Q_{bf}$, when the long-term bedload rates are controlled by frequent intermediate discharges (Andrews, 1980; Andrews & Nankervis, 1995). However, in cases where larger events tend to control long-term bedload transport rates, Q_{eff} becomes larger than Q_{bf} (Emmett & Wolman, 2001; Orndorff et al., 2004).
3. In channel restoration design, discharges presenting a return time varying between 1 and 2 years, Q_{rt} , are often considered a reasonable approximation of Q_{rep} (Doyle et al., 2007).

The event-based transport capacity, $Q_{s, rep}$, is then calculated for each definition of Q_{rep} using equation (4). By definition, it is not possible to compute the long-term transport capacity of a gravel bed river using only the representative discharge. Therefore, the estimation of the long-term transport capacity using any definition of representative discharge would need correction by a scaling factor, f_{rep} (e.g., Paola et al., 1992; Wright & Parker, 2003):

$$\overline{Q_{s, rep}} = f_{rep} Q_{s, rep}, \quad (10)$$

where f_{rep} is not known a priori and can be calculated as the ratio between $\overline{Q_s}$ (equation (8)) and $Q_{s, rep}$. In the following work, we study how the transport capacity computed with the three definitions of the representative discharge (Q_{eff} , Q_{bf} , and Q_{rt}) is influenced by riparian vegetation and discharge variability. We then assess how the single discharge approximation (equation (10)) compares to the exact solution of $\overline{Q_s}$ (equation (8)) and the sensitivity of f_{rep} to discharge variability.

2.4. Width Measurements on Natural Cases

Our model predictions offer new insights into the controls on widening/narrowing of rivers in response to change in confinement due to valley geometry (gorge vs. open valley) or vegetation (Figure 1). We compare these predictions with natural rivers located in New Zealand, Taiwan, and the Himalayas (see Figures S8 and S9). They were chosen according to two criteria (i) no major tributary should modify discharge and sediment supply to the main channel; (ii) the gorge section should have a continuous alluvial cover. The first criterion ensures that width is the only geometrical characteristic that varies alongstream, and the second ensures that the river is at or close to transport capacity. The measurements follow the method of Fisher et al. (2012). The active channel part where vegetation is not present is delineated using high-resolution satellite imagery obtained from Google Earth, and an along stream width variation is generated. A mean width and standard deviation is computed from measurements every 5 m along a 1-km reach in both the confined and unconfined section. We used SRTM or ALOS 30-m DEM data to estimate the ratio of the gorge slope to the braided slope in the sections where width was estimated. We found slope ratio between 0.86 and 1.04, with four out of seven rivers having less than 5% variation in slope (see Table S1).

3. Results on Spatially Uniform Valley Confinement and Vegetation for Single-Thread Channels

We start by comparing event-based transport capacity of confined and unconfined single-thread channels with different floodplain friction coefficients. We then integrate these calculations in different climatic contexts controlled by the frequency of extreme discharge events to compute $\overline{Q_s}$. Finally, we study the sensitivity of the effective discharge to vegetation and high-discharge frequency. This section only addresses the case of single-thread channels without any downstream changes in confinement or channel morphology. The latter case is examined in section 3.

3.1. Event-Based Impact of Riparian Vegetation on Sediment Transport

Channel shear stress is calculated for different floodplain friction coefficients and for the complete range of discharges (Figure 4). Below Q_{bf} , shear stress scales with discharge to the 0.6 power, corresponding to that of a rectangular channel with a Manning friction law (e.g., Whipple & Tucker, 1999). Above the bankfull discharge and for unconfined single-thread configurations, bed shear stress is reduced compared to the confined channel because flows spill onto the floodplain. For a discharge 100 times larger than the mean discharge, bed shear stress is ~100% larger in a confined channel than in the unconfined case without vegetation. As floodplain friction increases due to the density or type of vegetation present, bed shear stress increases due to the additional resistance yielding higher flow depths. Figure 4 shows that with increasing

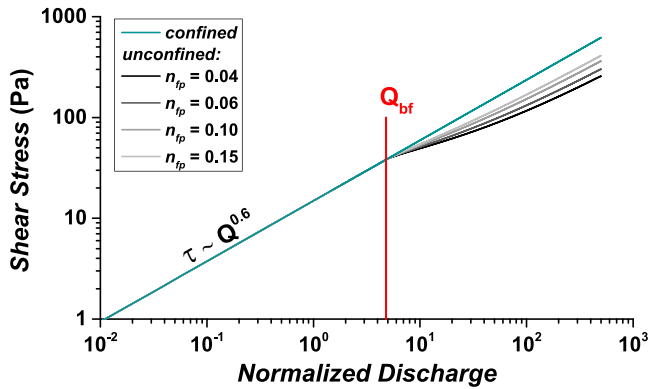


Figure 4. Bed shear stress exerted in the channel (τ) as a function of the normalized discharge for different floodplain friction values. The bankfull discharge corresponds to a normalized discharge of ~ 5 (i.e., 5 times the mean discharge).

$Q^{1.5}$), and the amplification of transport capacity increases continuously with discharge (Figure 5b). During moderate floods ($Q^* < 30$), the increase in suspended load transport capacity is negligible while bedload transport capacity can be doubled for the highest friction case. Only during rare and very large events ($Q^* > 100$) does vegetation increase the suspended load capacity as much as the bedload capacity. This highlights a striking difference on the sensitivity of the transport mode to vegetation for frequent floods.

Confinement of the channel has an even greater effect than vegetation. Bedload transport capacity can be increased up to 5 times due to confinement (Figure 5a) and suspended load up to nearly 10 times during extreme and rare events ($Q^* > 500$, Figure 5a). These results show noteworthy differences in the transport capacity of alluvial rivers and bedrock gorges simply as a function of channel confinement, with all other parameters being equal (slope, channel width, and grain size).

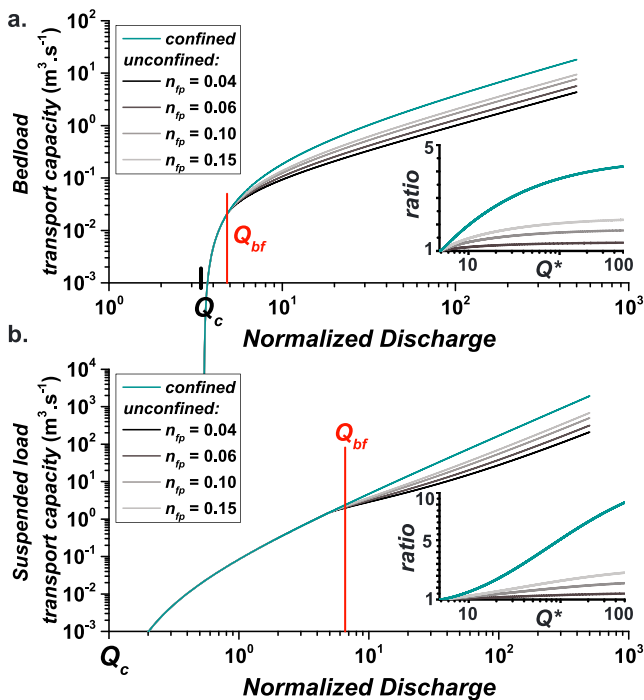


Figure 5. Sediment transport capacity as a function of the normalized discharge. The cyan plots represent sediment fluxes for a confined channel. (a) Bedload transport rate. (b) Suspended load transport capacity. Inserts show the ratio of transport capacity with respect to the unconfined case with uniform friction (i.e., $n_{ch} = n_{fp} = 0.04$).

floodplain friction, results asymptotically converge toward the confined (gorge) case. This illustrates the virtual confinement generated by dense floodplain vegetation.

The amplification of channel bed shear stress due to floodplain vegetation compared to a bare floodplain configuration (Figure 4) results in an increase of sediment transport capacity for a given overbank discharge event (Figure 5). Bedload and suspended load exhibit different sensitivities to river discharge due to the type of nonlinearity emerging from the exponent between transport capacity and shear stress (MPM vs. EH). For bedload, the scaling between transport capacity and discharge is asymptotically linear ($Q_{BL} \sim Q$, e.g., Tucker, 2004) beyond the critical discharge that is the main source of nonlinearity at discharges close to Q_{bf} ($Q_{BL} \sim Q^m$, with $m > 1$; Figure 5a). Consequently, the amplification of transport capacity increases rapidly above bankfull discharges compared to a bare floodplain and remains constant for very large floods. For suspended load, the nonlinearity emerges from the scaling exponent ($Q_{SL} \sim$

3.2. Impact of Discharge Variability and Floodplain Roughness on Long-Term Sediment Transport

Here we explore how floodplain vegetation modifies long-term sediment transport capacity under conditions of variable discharge. Following the approach of Wolman and Miller (1960), we plot the product of sediment transport capacity and event probability of occurrence to explore the contribution of various discharges to the overall long-term transport capacity budget (Figures 6a and 6b).

Bedload transport combines two characteristics promoting the action of events greater than or equal to Q_{bf} on long-term transport capacity: (i) a large critical shear stress and (ii) competent discharges starting slightly below Q_{bf} (Figure 5a). As discharge variability increases (i.e., k decreases), with a fixed channel geometry, overbank floods become more frequent and contribute more significantly to long-term sediment transport than events around Q_{bf} . This is highlighted by the effective discharge increasing from Q_{bf} at low variability ($k = 4$) to $1.5 \cdot Q_{bf}$ at very high variability ($k = 0.2$; Figure 6a). As floodplain vegetation only increases transport capacity for overbank floods (Figure 6a), the vegetation plays a significant role only when large floods are important in the long-term sediment budget. Hence, the amplifying effect of riparian vegetation on long-term bedload transport capacity increases with discharge variability (Figure 6c). For example, for a densely tree vegetated floodplain compared to a nonvegetated floodplain, the total long-term bedload capacity increases by 80% for $k = 0.2$, by 50% for $k = 1$, but only by 15% when $k = 4$ (Figure 6c).

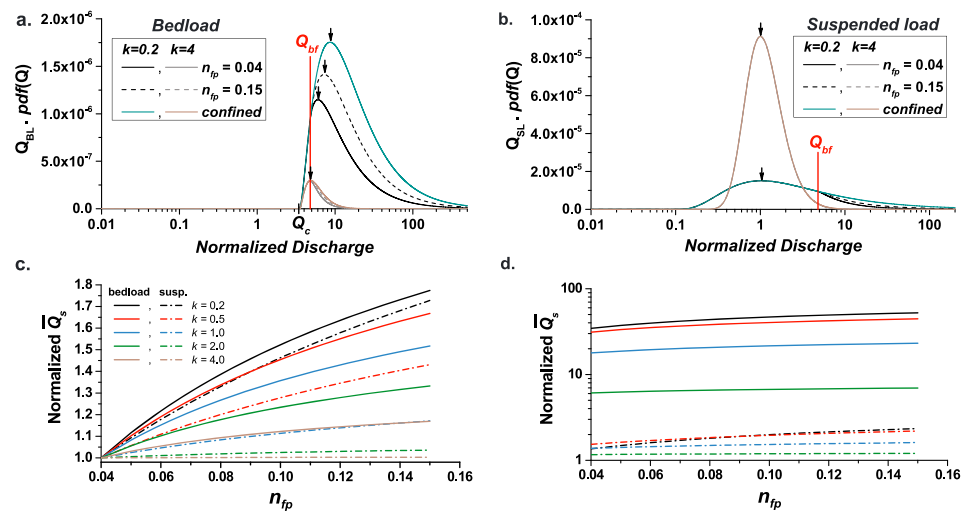


Figure 6. (a, b) Product of sediment transport capacity and event probability of occurrence ($pdf(Q^*)$). The effect of high-discharge frequency, riparian vegetation, and confinement is explored for (a) bedload transport and (b) suspended load transport. Arrows show the effective discharge. (c, d) Normalized long-term transport capacity as a function of floodplain friction. (c) The normalization is made by dividing long-term sediment flux by the case with uniform friction (i.e., $n_{ch} = n_{fp} = 0.04$) to investigate the role of floodplain friction. (d) The normalization is made by dividing long-term sediment flux by the $k = 4.0$ case to explore the role of discharge variability.

The influence of valley confinement can be understood as the asymptotic behavior of the virtual confinement generated by floodplain vegetation. Figure 6a shows that valley confinement only has a large effect under high-discharge variability, in which case the effective discharge of a bedrock gorge can be twice that of an alluvial river with a bare floodplain, with all other parameters being equal (slope, width, and grain size). In low-discharge variability regimes ($k > 2$), a confined bedrock gorge and an alluvial river of similar width and slope would have only minor differences in long-term transport capacity.

However, the amplification by vegetation and confinement remains small when compared to the impact of increasing discharge variability: As shown in Figure 6d, in which the long-term transport capacity is normalized by its value calculated for $k = 4$ (low variability), bedload transport capacity experiences a ~40- to 50-fold increase when k decreases from 4 to below 1. By giving more weight to larger and rarer events, highly variable hydraulic regimes would (i) lead to much higher long-term bedload transport capacity and (ii) enhance the boosting effect of vegetation on total bedload transport capacity. This emphasizes that flood frequency has to be considered when evaluating long-term bedload transport capacity in alluvial and bedrock rivers, while floodplain vegetation is only important in high variability regimes. These results also indicate that except for very low discharge variability (Figure 6a, $k = 4$), the effective discharge for bedload transport capacity in an alluvial river is expected to be 20% to 120% larger than the bankfull discharge and to depend on discharge variability and vegetation.

Contrary to bedload, the long-term budget of suspended load transport is mainly controlled by discharges lower than bankfull due to the very low critical discharge (Figure 6b). The effective discharge for suspended load is 5 to 10 times smaller than that for bedload and typically of the same order as the mean discharge. Therefore, extreme events have only a limited impact on long-term transport capacity. Consequently, the influence of discharge variability, riparian vegetation, and valley confinement is much smaller than in the bedload case: Suspended load transport capacity increases by a factor of only ~2 when k decreases from 4 to 1, while bedload increases by a factor of 50 (Figure 6d). Similarly, floodplain vegetation only increases suspended load capacity by a maximum of 70% in extreme variability regimes and for the highest friction. Otherwise, it has a negligible effect (i.e., <10%) for $k > 1$. This highlights the role of transport threshold in setting the dominance of large events on long-term transport compared to the scaling exponent of transport capacity laws. We note that the effective discharge for suspended load is much smaller than for bedload material, which raises the issue of the adequacy of using a constant reference discharge to model both bedload and suspended load transport in numerical simulations.

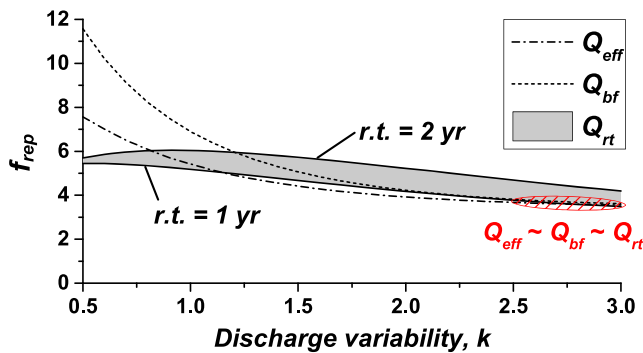


Figure 7. Influence of discharge variability on the scaling factor f_{rep} for different representative discharge definitions ($r.t.$ = return time, here equal to 1 and 2 years).

3.3. Representative Discharges for Bedload Transport and Discharge Variability

Long-term river evolution is generally studied or modeled using a representative discharge Q_{rep} for which three definitions have been proposed. We do not know whether this representative discharge should vary with climate variability or if a simple definition can be chosen that would systematically provide an adequate description of the exact long-term flux.

We first note that for any definition of Q_{rep} , $Q_{s, rep}$ always increases with discharge variability:

1. If $Q_{rep} = Q_{bf}$, the bankfull transport capacity is independent of k , but its frequency increases when k decreases.
2. If $Q_{rep} = Q_{eff}$, Q_{eff} and its associated frequency increase with k (Figure 6a).
3. If $Q_{rep} = Q_{rt}$, the annual frequency of Q_{rt} is fixed (to 1 or 0.5), but discharges that corresponds to that frequency always increase with k .

Figure 7 shows the ratio between $\overline{Q_s}$ (equation (8)) calculated using the complete discharge spectrum and $Q_{s, rep}$ computed with Q_{eff} , Q_{bf} , and Q_{rt} (equation (9)). This ratio is evaluated for different discharge variability. $Q_{s, rep}$ is systematically smaller than $\overline{Q_s}$ by a factor 3.5 to 11.5 depending on the definition of the representative discharge and the variability. Discrepancies between $\overline{Q_s}$ and $Q_{s, rep}$ increase with discharge variability (low k). In highly variable regimes, the discharge range controlling $\overline{Q_s}$ expands and have more weight compared to $Q_{s, rep}$, the value of which depends on only one discharge. When $k > 2$, f_{rep} shows limited variation, and the three representative discharges overlap ($Q_{eff} \sim Q_{bf} \sim Q_{rt} = 1$). Arguably, for this low variability regime, it is possible to assume that the representative discharge does not vary with climate variability. A correcting factor that will depend on the specific channel geometry and grain size must be introduced to accurately compute the long-term sediment flux with a single representative discharge weighted by its frequency of occurrence (in our test case, this factor is about 4). For $k < 1.5$, f_{rep} varies between 6 and 12, and there are significant differences between the three definitions of the representative discharge. The fixed return time discharge exhibits a reduced sensitivity to discharge variability (between 4 and 6). Therefore, using the fixed return time discharge to predict long-term bedload transport capacity whatever the discharge variability is the less biased solution compared to the other two definitions. The effective discharge Q_{eff} or the bankfull discharge Q_{bf} introduces an important underestimation of long-term transport capacity that increases with discharge variability. This makes using them arguably more complex and biased than the exact solution accounting for the whole discharge spectrum.

4. Results on Channel Widening Downstream of Confined Valleys

4.1. Results for Confined Versus Unconfined Single-Thread Channels With Differing Degrees of Floodplain Roughness

A direct consequence of the effect of valley confinement or *virtual* confinement by vegetation is that for an identical channel width, slope, and grain size, rivers can experience a significant drop in long-term bedload transport capacity when the confinement decreases (Figure 5). Figure 8 shows the reduction of bedload transport capacity experienced by a single-thread alluvial river with varying floodplain friction compared to a confined bedrock gorge of identical width ($W_{conf} = W_{ch}$), slope, and grain size. Two trends appear: First, the loss of transport capacity in the unconfined alluvial reach increases with discharge variability, reaching 40–60% for $k < 1$, but is limited to 20–25% for $k = 4$; second, the presence of vegetation attenuates the loss of transport capacity in highly variable flow regimes. We note that approaching this problem by assuming a spatially uniform representative discharge such as the bankfull discharge in the alluvial section would predict no transport capacity change.

If the river dynamics are transport limited, that is, bedload sediment transport is close to capacity, a negative alongstream gradient of transport capacity develops at the location of confinement loss driving aggradation over the long term. In a steady configuration, such total transport capacity gradients cannot

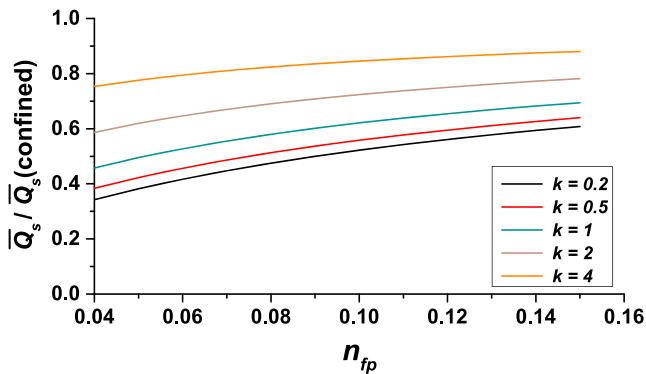


Figure 8. Long-term transport capacity of an unconfined alluvial reach normalized by that of a confined bedrock gorge as a function of floodplain friction.

be maintained. Channel geometry has to change to compensate for the reduction in confinement and to maintain the total transport capacity. Hence, systematic covariations in channel geometry with changes in valley confinement or floodplain vegetation should be observed. We focus our analysis on the transition between bedrock gorges and alluvial reaches (Figure 1), rather than changes in floodplain vegetation as the former represents a very sharp, sustained change in valley confinement.

Considering the bedrock/alluvial transition, previous observations (e.g., Lavé & Avouac, 2001) combined with our analysis based on 6 rivers indicates that 4 rivers have slope variations of less than 5% between confined and unconfined sections and 3 have up to 14% steeper braided reaches that could partially compensate for the loss of confinement (Table S1). This preliminary data set indicates a potential but limited role of slope in maintaining transport capacity when confinement decreases.

While surface grain size may vary longitudinally due to varying competent discharges, continuity of bedload sediment transport over the long term and in a steady state configuration implies that over the short distance considered in our analysis (less than a few kilometers), the bulk grain size distribution averaged through time should not vary abruptly. Hence, we suggest that channel width variation should be the dominant response of a channel to the loss of confinement at the transition between bedrock gorges and alluvial channels, except when the river slope in the gorge is lower than in the unconfined reach.

To test this assumption, we predict how channel width should vary in order for total bedload transport capacity to be maintained in the case that channel slope and grain size are identical in the confined and unconfined channels. First, we briefly report on a study of natural examples in three worldwide locations (Southern Alps of New Zealand, Himalayas, and Taiwan). This preliminary analysis only aims to identify the range of widening factor at bedrock/alluvial transitions, not to explore causal relationships with discharge variability, slope, grain size, and other geomorphological factors that are not well constrained. Second, we recall how total transport capacity varies with channel width in a stochastic threshold framework (Lague, 2014), as it is central to understanding the results. We subsequently explore the predictions of our simplified model considering unconfined single thread and braided rivers (Figure 1).

Changes in confinement or vegetation are very often correlated to changes in bank resistance (from bedrock to alluvium or with root reinforcements by vegetation). Such changes in bank resistance have often been invoked to explain changes in channel width for instance (Millar, 2000; Nicholas, 2013; Tal & Paola, 2007). In the following, we only consider the role of confinement loss to evaluate if it can explain observed variations in channel width or the transition to a braided system. Limits to this approach are addressed in the discussion section, including the potential role of channel slope changes downstream of the gorge.

4.2. Constraints on Widening From Natural Examples

We choose cases in which a continuous alluvial cover of sediment exists in the bedrock gorge, indicative of a system at, or close to, transport capacity. Figure 9 shows that mean channel width increases by a factor of 3 to 8 at the confined/unconfined transition. While the width in the confined gorge generally exhibits little variability (~15%), the active channel width in the unconfined alluvial part varies significantly over the 5–10 km chosen to compute the mean width. This translates into large fluctuations of the widening factor around the mean (Figure 1). We note that all rivers studied here are braided in unconfined sections, and single thread in the gorge. In this data set, only the Waiiau exhibits a steepening of the channel when the river emerges from the gorge.

4.3. Dependency of Long-Term Transport Capacity on Channel Width

The long-term total transport capacity, \overline{Q}_s , of an alluvial channel is the product of channel width and the unit transport capacity (i.e., $\overline{Q}_s = Wq_s(W)$). In the traditional constant effective discharge approach, \overline{Q}_s is subject

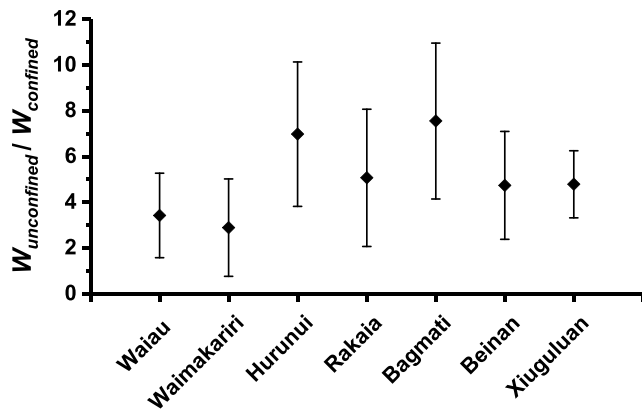


Figure 9. Ratio between unconfined and confined channel width for different natural rivers. Uncertainties derive from the standard deviation of width measurement distributions.

effect of the critical discharge variation with W is actually a dominant control over the long-term sediment transport rather than the reduction of shear stress available for transport at individual discharges. The resulting effect is that \bar{Q}_s decreases systematically with width, at a rate that decreases with discharge variability. Results shown in Figure 10 slightly differ from analytical predictions by Lague (2014) (Figure S1) because we use a more complete numerical solution with the inverse gamma distribution of daily stream flows alongside slightly different unit sediment transport law. In particular, the model results predict that \bar{Q}_s does not vary at small widths because the threshold is negligible. This regime is never met for gravel bed rivers and explains the difference with the analytical approximation proposed by Lague (2014), which assumes a non-negligible threshold.

The previous results have two important consequences: First, there is a fundamental difference in how the width in combination with the critical bedload shear stress affects long-term transport capacity between a constant effective discharge and an exact stochastic solution. Second, and this is an essential prediction, the stochastic predictions show that the decrease in transport capacity due to the loss of confinement at the bedrock/alluvial transition could only be compensated by a narrowing of the alluvial channel if it stays single threaded. This contradicts observations from Figure 8. However, the prediction holds only for single-thread rivers. In all studied natural cases, the alluvial channel becomes braided after the gorge exit (see Figures S8 and S9), which calls for using a flow geometry consistent with this type of river.

4.4. Prediction of Widening Factors With a Braiding Geometry

Here we explore whether solutions exist in which widening of the active channel can be predicted between a confined bedrock channel and an unconfined braided river. The slope ($S = 0.4\%$), the median grain size ($D_{50} = 10$ cm), and the Manning friction coefficient ($n_{ch} = 0.04$) are identical between the confined and the unconfined reach. According to the braided river geometry built following the description in section 2.1.2, the flow concentrates in the larger channel at low discharges. As the discharge increases, the smaller channels are activated and start to contribute to the total transport capacity once their shear stress overcomes the threshold of motion. During flooding conditions (i.e., $Q > Q_{bf}$), water inundates the active channel but remains restricted to the total width of the braid plain (W_{tot}). Large daily flows that inundate the total width of the braid plain can be high enough to initiate transport on the interbraid part. Therefore, the whole width of the braid plain is included in the total long-term transport capacity computations. The total transport capacity of the cross section is computed by integrating the local transport capacity over the entire width of the braid plain where the shear stress is above the critical shear stress. We compute the widening factor (W_{tot}/W_{conf}) by assuming that the total long-term bedload transport capacity must be identical between the braided alluvial section and the confined bedrock gorge. We first compute the total transport capacity in the braid plain for various k . We then numerically search for the confined channel width W_{conf} by minimizing the difference between the total long-term transport capacity of the unconfined and confined sections. We have checked that this problem has a unique solution for which the total long-term transport capacities are within 1% of each other.

to two opposite effects: It increases linearly with W through the integration over the channel section but decreases due to shear stress decreasing with W (i.e., $q_s \sim W^{0.9}$ when $\tau > \tau_c$ for a confined rectangular channel with a Manning friction law). The resulting total transport capacity should slightly increase with width as $\bar{Q}_s \propto W^{0.1}$ when $\tau \gg \tau_c$ (Figure 10; Lague, 2014). However, when considering bedload transport, the threshold is never negligible, and the resulting effect is that \bar{Q}_s decreases strongly with channel width until $\tau \leq \tau_c$ for which $\bar{Q}_s = 0$ (Figure 7; Croissant et al., 2017).

A stochastic approach using the complete spectrum of discharge yields significant differences compared to the constant discharge solution (Figure 10). The main reason is that a third effect plays out in modulating \bar{Q}_s : Width variations not only affect the shear stress for all discharges but also change the critical discharge Q_c at which bedload transport starts (Lague, 2014; Tucker & Bras, 2000). As channel width increases, Q_c increases, and the range of competent discharge decreases. The censoring

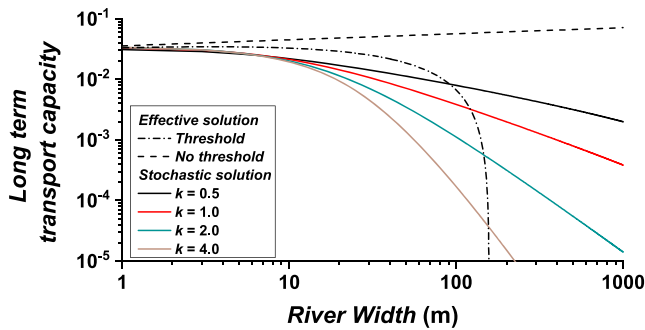


Figure 10. Predicted sensitivity of total long-term transport capacity to changes in channel width for a confined channel in the case of a constant discharge solution (with and without entrainment threshold; equation (9)), and comparison with the exact solution obtained by a stochastic approach accounting for the full spectrum of daily stream flows (equation (7)) (modified from Lague, 2014). Parameters used are shown in Table 2. A correction factor of 5 is applied to the constant discharge prediction to match the stochastic prediction as discussed in section 2.3 and shown in Figure 7.

Figure 11a shows that the modeling approach finds a solution with a widening ratio (W_{tot}/W_{conf}) spanning values from 2.2 to 8, which is consistent with observations. W_{tot}/W_{conf} systematically increases with k with values around 2.5 for high-discharge variability, and up to 8 for low-discharge variability. The ratio W_{tot}/W_{conf} decreases as the proportion of the interbraid bars reduces from 125% to 50% of the total braid plain width. Reducing the proportion of bars increases the confinement of the braid plain, in turn decreasing the width difference between the gorge and the braid plain. In all models the predicted bedrock gorge channel width is systematically larger than the individual braids. For instance, the bedrock gorge width is 4.7 times the largest thread of the braided river when $k = 1$ and 2.1 times for $k = 3$.

To better understand these results and the sensitivity to discharge variability, Figure 11b shows the product of the total transport capacity and the event probability of occurrence for both the braided river and bedrock gorge case. The same total long-term bedload transport capacity is achieved fundamentally differently in the gorge and braid plain sections; the sediment is entrained at a lower critical discharge in the narrow alluvial braids than in the wider confined section. Transport is thus more frequent in the alluvial section to compensate for the reduced effectiveness of large overbank floods due to the loss of confinement. This is illustrated by the mode of $Q_s \cdot pdf(Q)$ being offset to lower discharges in the braided section compared to the confined one (Figure 11b). As discharge variability modulates the contribution of large daily discharges to long-term transport, transport has to be less frequent, and the critical discharge higher in the gorge for high-discharge variability ($k = 1$) than for a low-discharge variability ($k = 3$). For $k = 1$, a second mode appears at $Q \sim 5,000 \text{ m}^3/\text{s}$ due to the added contribution of small braids set high on the floodplain to the total transport capacity.

Interestingly, an alongstream transport capacity gradient exists at the event scale for all solutions (Figure 11b): During frequent flooding, erosion should occur at the vicinity of the confined/unconfined transition due to a positive capacity gradient, while aggradation should occur during very large infrequent floods. Yet, over the long term, these differences average out, and no gradient in temporally averaged bedload transport capacity exists.

These results demonstrate the possibility of matching long-term bedload transport capacity in systems of significantly different width and confinement with a fully stochastic approach. This offers new insights into the controls on the large river widening observed downstream of bedrock gorges and alluvial channels, and the tendency to develop braided rivers that are discussed below.

Table 2
Model Parameters Used in the Transport Capacity Calculations for the Single-Thread and Braided River

Parameters	Units	Notation	Single thread	Braided river
Bankfull discharge	m^3/s	Q_{bf}	500	385
Median grain size	m	D_m	0.05	0.10
Channel width	m	W_{ch}	82	10–100
Cross-section total width	m	W_{tot}	482	1000
Slope	-	S	0.0013	0.004
Bank height	m	dh	3.13	0.3–1.6
$Q_{bankfull}/Q_{mean}$	-	Q_{bf}/Q_m	4.8	4.8
$\tau_{bankfull}/\tau_c$	-	τ_{bf}/τ_c	1.2	1.2
Norm. Discharge range	-	-	0.01–500	0.01–500
Channel friction	$\text{m}^{1/3} \cdot \text{s}$	n_{ch}	0.04	0.04
Floodplain friction	$\text{m}^{1/3} \cdot \text{s}$	n_{fp}	0.04–0.15	0.04
Discharge variability	-	k	0.2–4.0	0.5–4.0

Note. The use of hyphen “-” means that the variable is nondimensional.

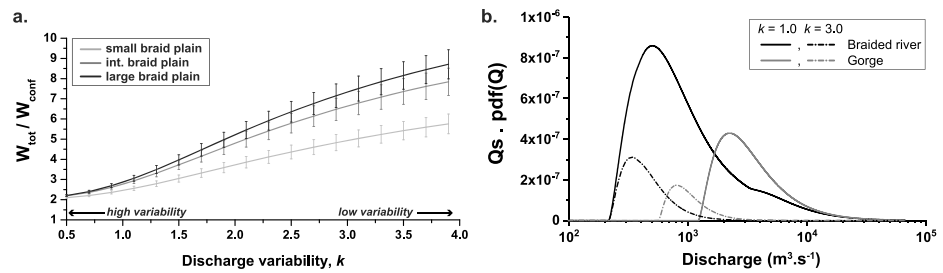


Figure 11. (a) W_{tot}/W_{conf} as a function of discharge variability for several braid plain configurations, presenting varying proportion of interbraid width. The “small braid plain” case corresponds to 50%, “int.” to 100%, and “large” to 125% of the cumulative width of braids. The bars represent the variability of the results emerging from the random generation of braid plains (here 50 braided geometries are generated for each value of k). (b) Product of sediment transport capacity and event probability of occurrence for confined and unconfined channel configuration. For each k , the graphs show the case where confined and unconfined long-term transport capacity are equal; that is, the integrals of the black and blue graphs are equal.

5. Discussion

5.1. Limitations

One of the first simplifications made in this study is the rectangular channel cross section that we impose for the single-thread channel, which is rarely seen in natural systems either for alluvial or bedrock rivers (Lague, 2014; Whipple et al., 2013). Our choice is consistent with the geometry used by Parker et al. (2007) and allows us to define a representative bankfull geometry. Moreover, tests performed on trapezoidal channels having large basal width and bank angles $>60^\circ$ show that the scaling between water discharge and flow depth (and thus shear stress) does not differ substantially from that of a rectangular channel (see Figure S4). More complex geometries and different bank angles would alter the scaling between shear stress and discharge (if the basal width is low compared to the total width; e.g., Turowski, Hovius, Meng-Long, et al., 2008; Turowski, Hovius, Wilson, et al., 2008). However, the consequences for long-term bedload transport capacity would be limited due to the dominance of over or near bank discharges on the long-term budget. For suspended load, a reduced exponent of the scaling relationship between shear stress and discharge for $Q < Q_{bf}$ would predict even less sensitivity to discharge variability than our current results. Given that we demonstrate that discharge variability has a limited impact on long-term suspended load, this would just reinforce this conclusion.

Another assumption of our approach is the constant slope between the confined channel and the unconfined channel. This assumption is verified in the majority of the natural examples we have studied, but in some rivers, the unconfined channel is steeper than the preceding bedrock gorge offsetting the reduction of long-term transport capacity due to the loss of confinement. A sensitivity analysis of model results shows that a steepened single-thread unconfined channel would not produce the range of widening ratios measured for natural cases (see Figure S5). However, when considering the braided model, our results show that the slope gradient has an influence on the predicted W_{tot}/W_{conf} ratio. The lower slope of the bedrock gorge is compensated for by a narrower channel to match the long-term transport capacity of the braided reach. W_{tot}/W_{conf} thus increases when the unconfined section is steeper than the gorge. The opposite happens when the bedrock gorge slope is steeper than the braided reach. Slope variations are thus expected to alter the widening ratio, but within the slope ratio variations explored here ($\pm 20\%$), river widening and the transition to a braided system is expected to be the most geometrically significant change of the river to compensate for the loss of confinement. Recall that the model assumes transport-limited conditions across the gorge. It cannot be applied to predict geometry when the bedrock gorge is significantly undercapacity, in which case detachment-limited conditions are expected to apply.

In our channel configuration, the floodplain width can be thought of as the maximal lateral distance that water can reach during a high-discharge event. This distance is expected to vary with vegetation density and the subtle microtopography of the floodplain. For a given overbank discharge, a wider floodplain lowers water depth, reduces channel transport capacity, but also enhances the sensitivity to differential friction and discharge variability. A sensitivity analysis (see Figure S6) shows that the floodplain width only matters

in high variability regimes ($k < 1$). In that case, a larger floodplain reinforces the amplification effect of riparian vegetation but reduces the impact of discharge variability. While the actual long-term bedload transport capacity is modified, our conclusions on the sensitivity to vegetation or discharge variability are not altered.

In a stochastic context, any prediction of long-term bedload transport for single thread channels will be sensitive to the transport threshold, which is set in our modeling framework by τ_{bf}/τ_c (Lague, 2014; Tucker & Bras, 2000). Increasing the threshold translates into a greater contribution of overbank discharges to the long-term transport capacity budget and a higher sensitivity to vegetation friction and discharge variability. To ensure generality of our results for various single-thread rivers, we choose a channel geometry set by $\tau_{bf}/\tau_c = 1.2$ as in Parker et al. (2007). We note however that for single-thread gravel bed rivers, τ_{bf}/τ_c ranges from 1.2 to 1.6 (Andrews, 1984; Dade & Friend, 1998; Parker et al., 2007). It has also been observed that vegetation through bank strengthening could increase τ_{bf}/τ_c toward values of around 2 (Millar, 2005; Pfeiffer et al., 2017). More recent studies have shown that the τ_{bf}/τ_c ratio could reach values larger than 2 but that a range of 1 to 2 encompasses the central tendency of values for gravel bed rivers (Buffington, 2012). A sensitivity analysis (see Figure S7) shows that our conclusions hold for τ_{bf}/τ_c between 1.2 and 2. The lower the value of τ_{bf}/τ_c , the greater is the sensitivity to vegetation and discharge variability.

The synthetic reproduction of braided channel geometry is a difficult endeavor as shown by the complexity of natural cases (Figure 1). However, the new simplified geometrical model that we introduce successfully reproduces empirical observations. This success is not random, as the model reproduces observations for a narrow range of parameters and simpler models using a series of rectangular braids are not able to capture the variation of the wetted area of braided rivers with discharge.

5.2. Impact of Discharge Variability on the Transport Capacity of Alluvial Rivers and Their Morphodynamics

Our results show that discharge variability has a very large impact on long-term bedload transport capacity (Figure 6c) for a given channel geometry, while it is expected to have a minor effect on suspended load. As such, it is an essential element to factor in models of long-term river morphodynamics, in particular under varying climatic forcing. For computational reasons, it remains challenging to fully capture the impact of a large spectrum of discharge in 2-D river morphodynamics models, such that an effective discharge, sometime slightly varying, is generally used (e.g., Croissant et al., 2017; Davy & Lague, 2009; Nicholas, 2013). Yet, as shown by the example of the bedrock/alluvial transition, considering discharge variability is not only essential to capture correctly the effect of a variable river hydrology, and in particular the extremes, but also to unravel new relationships between channel equilibrium geometry and boundary conditions that constant discharge approaches cannot capture.

One expects equilibrium channel geometry to vary significantly with discharge variability due to the large impact on bedload transport capacity. Disentangling the specific effect of discharge variability among other boundary conditions such as grain size, sediment supply, mean discharge, and bank resistance is difficult. A first step in that direction has been obtained by Phillips and Jerolmack (2016) who have shown that a large number of rivers in the United States covering a wide range of discharge variability regimes tend to be organized such that bankfull shear stress is $\sim 20\%$ higher than critical shear stress. This observed apparent self-organization of rivers to a threshold state (Parker et al., 2007; Talling, 2000) despite large variations in discharge variability shows that channel equilibrium geometry is indeed varying significantly with discharge variability. This result is consistent with the strong influence of discharge variability on transport capacity for a fixed channel geometry. Phillips and Jerolmack (2016) also observed that the effective discharge (defined as Q_{bf}) was a frequent event, a result that is consistent with our model prediction for alluvial rivers (Figure 6a), where the effective discharge, even for extremely large variability ($k = 0.2$), remains a frequent discharge (Q_{eff}/Q_{bf} ranging between 1 and 2). This originates from the strong reduction in shear stress/discharge scaling during flooding and the limited asymptotic nonlinearity of the bedload transport law. Yet our results show that even if the effective discharge is a frequent event, because the threshold of transport is high, any small change in variability changes significantly the frequency of competent discharge and the long-term bedload transport capacity in a larger way than the effective event does.

5.3. New Insights on Channel Widening at the Bedrock Gorge/Alluvial Plain Transition

The modeling results show that the loss of confinement downstream of bedrock gorges would translate into a significant loss of transport capacity if the slope and grain size were uniform. This condition could not be sustained over the long term and would require a change in channel geometry. We demonstrate that the narrow threads in a braided river presenting a lower critical discharge than in the confined gorges increase the range of competent discharge and ultimately compensate for the loss of confinement experienced during high flow. As such, braided rivers appear to be the optimal geometric response to the problem of increasing the range of competent discharges and can be viewed as a river morphodynamic response to maintain along-stream transport capacity. Therefore, while braid geometry (trapezoidal cross section) impacts the scaling between discharge and transport capacity, the mechanisms by which a braid plain increases its transport capacity is by the added effect of narrower threads. Here, the change in cross-section shape from the gorge (rectangular) to the braid plain (trapezoidal) does not significantly impact the results as discussed above (see Figure S4).

The modeling results also reveal new insights regarding alluvial bed dynamics over short and long time-scales near the transition between narrow bedrock gorges and wide alluvial reaches due to alongstream variation in Q_c ; considering a single discharge event, the transport capacity would systematically vary downstream. The frequent and intermediate discharges promote erosion in the alluvial section due to the smaller Q_c , and large events drive aggradation due to the loss of confinement. Combined with the fact that the transition from bedrock banks to alluvial banks favors the lateral mobility of the flow, the temporal fluctuations in aggradation/degradation at gorge outlets may be of critical importance for the initiation and maintenance of the braiding instability. Our results also show how spatial variations in width and confinement can result in short-term dynamics that a constant discharge approach would qualify as unbalanced (as shown in Garcia Lugo et al., 2015), while the long-term integration of the complete spectrum of discharges is indeed balanced.

The previous analyses do not account for the effect of changes in bank resistance, which can promote river widening in the alluvial section but is still difficult to account for mechanically (Limaye & Lamb, 2014). A more systematic analysis of potential slope variations between the gorge and the braided part of natural rivers is also needed. Combined with field measurement of grain size and discharge variability, these data will help in getting a more complete picture of the variations of river geometry downstream of gorges. Our modeling results show that changes in river confinement are an integral part of the problem of channel narrowing in bedrock gorges that are traditionally interpreted as being related to localized uplift and/or a change in channel bank resistance (e.g., Lavé & Avouac, 2001; Turowski et al., 2009; Yanites et al., 2010). The effect of unconfinement should also be considered and will be greatest in areas of high-discharge variability, limited vegetation, and high fraction of bedload sediment supply.

5.4. Impact of Vegetation on the Transport Capacity of Alluvial Rivers

Our results demonstrate that for a typical single-thread gravel bed river, a dense floodplain vegetation generating high flow friction would increase long-term bedload transport capacity by a factor of up to 2 in conditions of high-discharge variability compared to a uniform friction condition. When discharge variability is low ($k > 2$), floodplain vegetation has a more subdued effect and would only have a significant impact (i.e., amplifying sediment transport by more than 10–20%) for the largest end-member of the studied friction ($n_p = 0.15$). Suspended load transport capacity is in general marginally increased by floodplain vegetation, except in the highest discharge variability regimes ($k < 0.5$) when it can be increased by 50%.

These results demonstrate that the virtual confinement offered by riparian vegetation can have a significant impact on bedload transport efficiency such that the equilibrium geometry would be expected to be different with or without riparian vegetation, but only if discharge variability is high enough. Under the assumption that floodplain vegetation only affects friction, rivers at steady state with an identical long-term bedload supply rates, similar slope, and grain size would have an equilibrium width that increases with the level of virtual confinement by vegetation. This results from the same mechanism at work in the bedrock/alluvial transition: more effective overbank discharges when vegetation is present have to be compensated for by a reduced range of competent discharge to match the total capacity of a bare floodplain configuration. This can only be obtained by a larger width that increases Q_c .

Yet this prediction does not factor in any influence of vegetation on bank resistance. It has been observed that riparian vegetation tends to reduce the width of single-thread rivers with otherwise similar boundary conditions (e.g., Camporeale et al., 2013; Millar, 2000, 2005; Parker et al., 2007). Increased bank resistance by root reinforcement has been put forward to explain such channel narrowing, as well as reduced near-bank flow velocities (Camporeale et al., 2013; Nicholas, 2013; Tal & Paola, 2007). Our modeling work neglects these important processes but suggests that riparian vegetation through virtual confinement could have a widening effect that would counteract channel narrowing due to vegetation induced bank erosion reduction. As a result the overall impact of vegetation on channel geometry could be more subdued than previously thought, especially in highly variable discharge regimes. As this effect can only be captured by considering the complete spectrum of discharges and is particularly important in high-discharge variability regimes, it has not emerged previously as a mechanism by which vegetation may influence channel morphodynamics, as most current models use either a constant representative discharge or slightly varying discharge (Camporeale et al., 2013).

5.5. Effective Discharge

Modeling river morphodynamics on long timescales can be done by simulating the complete spectrum of discharge (e.g., Lague, 2010) or by only one representative discharge event (e.g., Croissant et al., 2017; Davy & Lague, 2009; Nicholas, 2013). The latter is appealing and is generally chosen given the computational constraints on simulating all discharges. However, we have shown that underestimations of long-term transport capacity introduced by the use of representative discharge compared to a full description of the discharge range experienced by rivers vary between a factor of 3 to 12 depending on the representative discharge definition and the climatic conditions (discharge variability).

These errors have an impact on at-a-station transport capacity prediction but also on along stream predictions, especially when rivers experience significant geometry and regimes changes (from gorges to braided rivers for instance; e.g., Lavé & Avouac, 2001; Turowski et al., 2009; Yanites et al., 2010). In these cases, assuming a spatially uniform representative discharge is likely to be problematic, as the critical discharge and the peak of efficiency differ from unconfined to confined channels. Additionally, we have demonstrated that the discrepancies between representative discharges for suspended load and bedload render its use in numerical simulation more difficult, as one would have to adjust transport law parameters to compensate for the different effective discharges. Overall, our results advocate for a more systematic use of fully stochastic numerical models to avoid potential biases in using constant effective discharge models.

6. Conclusion

We present a simple model that computes the long-term transport capacity of rivers by incorporating a stochastic distribution of mean daily discharge events coupled with different sediment transport laws. The calculations are made on confined and unconfined cross sections in which geometries are constrained from empirical relationships based on data previously compiled for natural rivers. The different vegetation contexts are simulated by tuning the floodplain Manning friction coefficient, which increases with vegetation density and type. The flood frequency is modulated by a variability parameter that controls the relative contribution of extreme events compared to frequent ones.

The comparison between unconfined alluvial channels and confined bedrock gorges with identical width, slope, and grain size shows that the latter always have a larger total transport capacity due to valley confinement. Consequently, channel geometry has to vary at the unconfined alluvial/confined bedrock transition to maintain long-term transport capacity. Central to our analysis is the demonstration that total transport capacity decreases with greater channel width and that this relationship is sensitive to discharge variability. Consequently, we demonstrate that a braided alluvial channel made of inner channels that are comparatively smaller than the bedrock gorge can maintain the total alongstream capacity despite the loss of confinement due to a larger range of competent discharge (i.e., a smaller critical discharge).

Riparian vegetation increases event-based transport capacity significantly by raising water depth in the active alluvial channel and thus acts as a virtual confinement of the river. We found that long-term bedload transport capacity is only sensitive to riparian vegetation when discharge variability is high. Bedload

transport capacity increases significantly with discharge variability in relation to the high transport threshold that is typical of threshold-state channels.

Our stochastic modeling approach introduces a new dimension to the relationship between discharge, width, slope, grain size, and transport efficiency through the role of channel confinement and vegetation. Future work should focus on expanding this work with a 2-D morphodynamics model of river dynamics that is capable of reproducing a wide spectrum of discharge, accounting for changes in bank resistance, and is able to capture channel instabilities such as braiding. This would help in deciphering the relationship between equilibrium geometry and boundary conditions that can only be fully addressed by considering the full spectrum of stochastic hydraulic forcing occurring in natural rivers.

Acknowledgments

This research was funded by CNRS/INSU/ALEAS project SEDIQUAKE and Agence Nationale de la Recherche (ANR-14-CE33-0005) project EROQUAKE. The authors are grateful to Rob Ferguson, Murray Hicks, an anonymous reviewer, the associate editor, and the editor for their insightful comments that greatly improved the quality of the manuscript. We thank Rebecca Hodge for her comments and proofreading of the manuscript. All data used in the simulations are reported in the manuscript.

References

- Andrews, E. D. (1980). Effective and bankfull discharges of streams in the Yampa River basin, Colorado and Wyoming. *Journal of Hydrology*, *46*(3–4), 311–330. [https://doi.org/10.1016/0022-1694\(80\)90084-0](https://doi.org/10.1016/0022-1694(80)90084-0)
- Andrews, E. D. (1984). Bed-material entrainment and hydraulic geometry of gravel-bed rivers in Colorado. *Geological Society of America Bulletin*, *95*(3), 371–378. [https://doi.org/10.1130/0016-7606\(1984\)95<371:BEAHGO>2.0.CO;2](https://doi.org/10.1130/0016-7606(1984)95<371:BEAHGO>2.0.CO;2)
- Andrews, E. D., & Nankervis, J. M. (1995). In J. E. Costa, A. J. Miller, K. W. Potter, & P. R. Wilcock (Eds.), *Natural and anthropogenic influences in fluvial geomorphology*, *Geophysical Monograph Series*, (Vol. 89). Washington, D. C: American Geophysical Union. <https://doi.org/10.1029/GM089>
- Arcecent, G. J., & Schneider, V. R. (1989). *Guide for selecting Manning's roughness coefficients for natural channels and floodplains*. *USGS Survey Water Supply Paper*, *233*, 1–38.
- Ashmore, P. (2013). Morphology and dynamics of braided rivers. Editor in Chief. In J. Shroder & E. Wohl (Eds.), *Treatise on Geomorphology. Fluvial Geomorphology* (Vol. 9, pp. 289–312). San Diego, CA: Academic Press. <https://doi.org/10.1016/B978-0-12-374739-6.00242-6>
- Ashmore, P., & Sauks, E. (2006). Prediction of discharge from water surface width in a braided river with implications for at-a-station hydraulic geometry. *Water Resources Research*, *42*, W03406. <https://doi.org/10.1029/2005WR003993>
- Barry, J. J., Buffington, J. M., Goodwin, P., King, J. G., & Emmett, W. W. (2008). Performance of bed-load transport equations relative to geomorphic significance: Predicting effective discharge and its transport rate. *Journal of Hydraulic Engineering*, *134*(5), 601–615. [https://doi.org/10.1061/\(ASCE\)0733-9429\(2008\)134:5\(601\)](https://doi.org/10.1061/(ASCE)0733-9429(2008)134:5(601))
- Bertoldi, W., Ashmore, P., & Tubino, M. (2009). A method for estimating the mean bed load flux in braided rivers. *Geomorphology*, *103*(3), 330–340. <https://doi.org/10.1016/j.geomorph.2008.06.014>
- Bousmar, D., & Zech, Y. (1999). Momentum transfer for practical flow computation in compound channels. *Journal of Hydraulic Engineering*, *125*(7), 696–706. [https://doi.org/10.1061/\(ASCE\)0733-9429\(1999\)125:7\(696\)](https://doi.org/10.1061/(ASCE)0733-9429(1999)125:7(696))
- Bren, L. J. (1993). Riparian zone, stream, and floodplain issues: A review. *Journal of Hydrology*, *150*(2–4), 277–299. [https://doi.org/10.1016/0022-1694\(93\)90113-N](https://doi.org/10.1016/0022-1694(93)90113-N)
- Buffington, J. M. (2012). Changes in channel morphology over human time scales. In *Gravel-Bed Rivers: Processes, Tools, Environments*, (pp. 433–463). <https://doi.org/10.1002/9781119952497.ch32>
- Camporeale, C., Perucca, E., Ridolfi, L., & Gurnell, a. M. (2013). Modeling the interactions between river morphodynamics and riparian vegetation. *Reviews of Geophysics*, *51*, 379–414. <https://doi.org/10.1002/rog.20014>
- Casas, A., Lane, S. N., Yu, D., & Benito, G. (2010). A method for parameterising roughness and topographic sub-grid scale effects in hydraulic modelling from LiDAR data. *Hydrology and Earth System Sciences*, *14*(8), 1567–1579. <https://doi.org/10.5194/hess-14-1567-2010>
- Chow, V. T. (1959). *Open-channel Hydraulics* (680 pp.). New York, NY: McGraw-Hill.
- Cobby, D. M., Mason, D. C., Horritt, M. S., & Bates, P. D. (2003). Two-dimensional hydraulic flood modelling using a finite-element mesh decomposed according to vegetation and topographic features derived from airborne scanning laser altimetry. *Hydrological Processes*, *17*(10), 1979–2000. <https://doi.org/10.1002/hyp.1201>
- Crave, A., & Davy, P. (2001). A stochastic “precipiton” model for simulating erosion/sedimentation dynamics. *Computers & Geosciences*, *27*(7), 815–827. [https://doi.org/10.1016/S0098-3004\(00\)00167-9](https://doi.org/10.1016/S0098-3004(00)00167-9)
- Croissant, T., Lague, D., Steer, P., & Davy, P. (2017). Rapid post-seismic landslide evacuation boosted by dynamic river width. *Nature Geoscience*, *10*(9), 680–684. <https://doi.org/10.1038/ngeo3005>
- Dade, W. B., & Friend, P. F. (1998). Grain size, sediment transport regime, and channel slope in alluvial rivers. *The Journal of Geology*, *106*(6), 661–676. <https://doi.org/10.1086/516052>
- Darby, S. E. (1999). Effect of riparian vegetation on flow resistance and flood potential. *Journal of Hydraulic Engineering*, *125*(5), 443–454. [https://doi.org/10.1061/\(ASCE\)0733-9429\(1999\)125:5\(443\)](https://doi.org/10.1061/(ASCE)0733-9429(1999)125:5(443))
- Davy, P., & Lague, D. (2009). Fluvial erosion/transport equation of landscape evolution models revisited. *Journal of Geophysical Research*, *114*, F03007. <https://doi.org/10.1029/2008JF001146>
- Deal, E., Botter, G., & Braun, J. (2018). Understanding the role of rainfall and hydrology in determining fluvial erosion efficiency. *Journal of Geophysical Research: Earth Surface*, *123*, 744–778. <https://doi.org/10.1002/2017JF004393>
- DiBiase, R. A., & Whipple, K. X. (2011). The influence of erosion thresholds and runoff variability on the relationships among topography, climate, and erosion rate. *Journal of Geophysical Research*, *116*, F04036. <https://doi.org/10.1029/2011JF002095>
- Doyle, M. W., Shields, D., Boyd, K. F., Skidmore, P. B., & Dominick, D. (2007). Channel-forming discharge selection in river restoration design. *Journal of Hydraulic Engineering*, *133*(7), 831–837. [https://doi.org/10.1061/\(ASCE\)0733-9429\(2007\)133:7\(831\)](https://doi.org/10.1061/(ASCE)0733-9429(2007)133:7(831))
- Emmett, W. W., & Wolman, M. G. (2001). Effective discharge and gravel-bed rivers. *Earth Surface Processes and Landforms*, *26*(13), 1369–1380. <https://doi.org/10.1002/esp.303>
- Engelund, F., & Hansen, E. (1967). *A Monograph on Sediment Transport in Alluvial Streams*. Copenhagen, Denmark: Teknisk Forlag.
- Ferguson, R. (2010). Time to abandon the Manning equation? *Earth Surface Processes and Landforms*, *35*(15), 1873–1876. <https://doi.org/10.1002/esp.2091>

- Fernandes, J. N., Leal, J. B., & Cardoso, a. H. (2012). Flow structure in a compound channel with smooth and rough floodplains. *European Water Publications*, 38(1964), 3–12.
- Finnegan, N. J., Roe, G., Montgomery, D. R., & Hallet, B. (2005). Controls on the channel width of rivers: Implications for modeling fluvial incision of bedrock. *Geology*, 33(3), 229–232. <https://doi.org/10.1130/G21171.1>
- Fisher, G. B., Amos, C. B., Bookhagen, B., Burbank, D. W., & Godard, V. (2012). Channel widths, landslides, faults, and beyond: The new world order of high-spatial resolution Google Earth imagery in the study of earth surface processes. *Geological Society of America Special Papers*, 492(01), 1–22. [https://doi.org/10.1130/2012.2492\(01\)](https://doi.org/10.1130/2012.2492(01)).
- García Lugo, G. A., Bertoldi, W., Henshaw, A. J., & Gurnell, A. M. (2015). The effect of lateral confinement on gravel bed river morphology. *Water Resources Research*, 51, 7145–7158. <https://doi.org/10.1002/2015WR017081>
- Hunter, N. M., Bates, P. D., Horritt, M. S., & Wilson, M. D. (2007). Simple spatially-distributed models for predicting flood inundation: A review. *Geomorphology*, 90(3–4), 208–225. <https://doi.org/10.1016/j.geomorph.2006.10.021>
- Lague, D. (2010). Reduction of long-term bedrock incision efficiency by short-term alluvial cover intermittency. *Journal of Geophysical Research*, 115, F02011. <https://doi.org/10.1029/2008JF001210>
- Lague, D. (2014). The stream power river incision model: Evidence, theory and beyond. *Earth Surface Processes and Landforms*, 39(1), 38–61. <https://doi.org/10.1002/esp.3462>
- Lague, D., Hovius, N., & Davy, P. (2005). Discharge, discharge variability, and the bedrock channel profile. *Journal of Geophysical Research*, 110, F04006. <https://doi.org/10.1029/2004JF000259>
- Lavé, J., & Avouac, J. P. J. (2001). Fluvial incision and tectonic uplift across the Himalayas of Central Nepal. *Journal of Geophysical Research*, 106(B11), 26561. <https://doi.org/10.1029/2001JB000359-26591>.
- Leopold, L. B., Wolman, M. G., & Miller, J. P. (1964). *Fluvial processes in geomorphology*, U.S. Geol. Surv. Prof. Pap., (Vol. 522, p. 57).
- Limaye, A. B. S., & Lamb, M. P. (2014). Numerical simulations of bedrock valley evolution by meandering rivers with variable bank material. *Journal of Geophysical Research: Earth Surface*, 119, 927–950. <https://doi.org/10.1002/2013JF002997>
- Mason, D. C., Cobby, D. M., Horritt, M. S., & Bates, P. D. (2003). Floodplain friction parameterization in two-dimensional river flood models using vegetation heights derived from airborne scanning laser altimetry. *Hydrological Processes*, 17(9), 1711–1732. <https://doi.org/10.1002/hyp.1270>
- Meyer-Peter, E., & Müller, R. (1948). Formulas for bed-load transport. Proceedings of the 2nd Meeting of the International Association of Hydraulic Research, 39–64. doi:1948-06-07
- Millar, R. G. (2000). Influence of bank vegetation on alluvial channel patterns. *Water Resources Research*, 36(4), 1109–1118. <https://doi.org/10.1029/1999WR900346>
- Millar, R. G. (2005). Theoretical regime equations for mobile gravel-bed rivers with stable banks. *Geomorphology*, 64(3–4), 207–220. <https://doi.org/10.1016/j.geomorph.2004.07.001>
- Molnar, P., Anderson, R. S., Kier, G., & Rose, J. (2006). Relationships among probability distributions of stream discharges in floods, climate, bed load transport, and river incision. *Journal of Geophysical Research*, 111, F02001. <https://doi.org/10.1029/2005JF000310>
- Mueller, E. R., Pitlick, J., & Nelson, J. M. (2005). Variation in the reference Shields stress for bed load transport in gravel-bed streams and rivers. *Water Resources Research*, 41, W04006. <https://doi.org/10.1029/2004WR003692>
- Nicholas, A. P. (2000). Modelling bedload yield in braided gravel bed rivers. *Geomorphology*, 36(1–2), 89–106. [https://doi.org/10.1016/S0169-555X\(00\)00050-7](https://doi.org/10.1016/S0169-555X(00)00050-7)
- Nicholas, A. P. (2013). Modelling the continuum of river channel patterns. *Earth Surface Processes and Landforms*, 38(10), 1187–1196. <https://doi.org/10.1002/esp.3431>
- Orndorff, R. L., Glonek, L. A., Orndorff, L., & Glonek, L. A. (2004). Effective and bankfull discharge in Great Basin National Park, Nevada. *Journal of the Arizona-Nevada Academy of Science*, 36(2), 103–110.
- Paola, C. (1996). Incoherent structure: turbulence as a metaphor for stream braiding. In P. J. Ashworth et al. (Eds.), *Coherent Flow Structures in Open Channels* (pp. 705–723). Chichester: John.
- Paola, C., Heller, P. L., & Angevine, C. L. (1992). The large scale dynamics of grain size variation in alluvial basins, 1: Theory. *Basin Research* <https://doi.org/10.1111/j.1365-2117.1992.tb00145.x>, 4(2), 73–90.
- Parker, G., Wilcock, P. R., Paola, C., Dietrich, W. E., & Pitlick, J. (2007). Physical basis for quasi-universal relations describing bankfull hydraulic geometry of single-thread gravel bed rivers. *Journal of Geophysical Research*, 112, F04005. <https://doi.org/10.1029/2006JF000549>
- Petit, F., & Pauquet, A. (1997). Bankfull discharge recurrence interval in gravel-bed rivers. *Earth Surface Processes and Landforms*, 22(7), 685–693. [https://doi.org/10.1002/\(SICI\)1096-9837\(199707\)22:7<685::AID-ESP744>3.0.CO;2-J](https://doi.org/10.1002/(SICI)1096-9837(199707)22:7<685::AID-ESP744>3.0.CO;2-J)
- Pfeiffer, A. M., Finnegan, N. J., & Willenbring, J. K. (2017). Sediment supply controls equilibrium channel geometry in gravel rivers. *Proceedings of the National Academy of Sciences*, 114(13), 3346–3351. <https://doi.org/10.1073/pnas.1612907114>
- Phillips, C. B., & Jerolmack, D. J. (2016). Self-organization of river channels as a critical filter on climate signals. *Science*, 352(6286), 694–697. <https://doi.org/10.1126/science.aad3348>
- Pickup, G., & Warner, R. F. (1976). Effects of hydrologic regime on magnitude and frequency of dominant discharge. *Journal of Hydrology*, 29(1–2), 51–75. [https://doi.org/10.1016/0022-1694\(76\)90005-6](https://doi.org/10.1016/0022-1694(76)90005-6)
- Pitlick, J., & Cress, R. (2002). Downstream changes in the channel geometry of a large gravel bed river. *Water Resources Research*, 38(10), 1216. <https://doi.org/10.1029/2001WR000898>
- Powell, D. M. (2014). Flow resistance in gravel-bed rivers: Progress in research. *Earth-Science Reviews*, 136, 301–338. <https://doi.org/10.1016/j.earscirev.2014.06.001>
- Redolfi, M., Tubino, M., Bertoldi, W., & Brasington, J. (2016). Analysis of reach-scale elevation distribution in braided rivers: Definition of a new morphologic indicator and estimation of mean quantities. *Water Resources Research*, 52, 5951–5970. <https://doi.org/10.1002/2015WR017918>
- Rossi, M. W., Whipple, K. X., & Vivoni, E. R. (2016). Precipitation and evapotranspiration controls on daily runoff variability in the contiguous United States and Puerto Rico. *Journal of Geophysical Research: Earth Surface*, 121, 128–145. <https://doi.org/10.1002/2015JF003446>
- Rudorff, C. M., Melack, J. M., & Bates, P. D. (2014). Flooding dynamics on the lower Amazon floodplain: 1. Hydraulic controls on water elevation, inundation extent, and river-floodplain discharge. *Water Resources Research*, 50, 619–634. <https://doi.org/10.1002/2013WR014091>
- Ryan, S. E., & Emmett, W. W. (2002). The nature of flow and sediment movement in Little Granite Creek near Bondurant, Wyoming. *Forest Science*. <https://doi.org/10.2737/RMRS-GTR-90>

- Ryan, S. E., Porth, L. S., & Troendle, C. A. (2002). Defining phases of bedload transport using piecewise regression. *Earth Surface Processes and Landforms*, 27(9), 971–990. <https://doi.org/10.1002/esp.387>
- Simon, A., Dickerson, W., & Heins, A. (2004). Suspended-sediment transport rates at the 1.5-year recurrence interval for ecoregions of the United States: Transport conditions at the bankfull and effective discharge? *Geomorphology*, 58(1–4), 243–262. <https://doi.org/10.1016/j.geomorph.2003.07.003>
- Tabacchi, E., Lambs, L., Guilloy, H., Planty-Tabacchi, A.-M., Muller, E., & Décamps, H. (2000). Impacts of riparian vegetation on hydrological processes. *Hydrological Processes*, 14(16–17), 2959–2976. [https://doi.org/10.1002/1099-1085\(200011/12\)14](https://doi.org/10.1002/1099-1085(200011/12)14)
- Tal, M., & Paola, C. (2007). Dynamic single-thread channels maintained by the interaction of flow and vegetation. *Geology*, 35(4), 347. <https://doi.org/10.1130/G23260A.1>
- Talling, P. J. (2000). Self-organization of river networks to threshold states. *Water Resources Research*, 36(4), 1119–1128. <https://doi.org/10.1029/1999WR900339>
- Tsujimoto, T. (1999). Fluvial processes in streams with vegetation. *Journal of Hydraulic Research*, 37(6), 789–803. <https://doi.org/10.1080/00221689909498512>
- Tucker, G. E. (2004). Drainage basin sensitivity to tectonic and climatic forcing: Implications of a stochastic model for the role of entrainment and erosion thresholds. *Earth Surface Processes and Landforms*, 29(2), 185–205. <https://doi.org/10.1002/esp.1020>
- Tucker, G. E., & Bras, R. L. (2000). A stochastic approach to modeling the role of rainfall variability in drainage basin evolution. *Water Resources Research*, 36(7), 1953. <https://doi.org/10.1029/2000WR900065-1964>
- Turowski, J. M., Hovius, N., Meng-Long, H., Lague, D., & Men-Chiang, C. (2008). Distribution of erosion across bedrock channels. *Earth Surface Processes and Landforms*, 33(3), 353–363. <https://doi.org/10.1002/esp.1559>
- Turowski, J. M., Hovius, N., Wilson, A., & Horng, M.-J. (2008). Hydraulic geometry, river sediment and the definition of bedrock channels. *Geomorphology*, 99(1–4), 26–38. <https://doi.org/10.1016/j.geomorph.2007.10.001>
- Turowski, J. M., Lague, D., & Hovius, N. (2009). Response of bedrock channel width to tectonic forcing: Insights from a numerical model, theoretical considerations, and comparison with field data. *Journal of Geophysical Research*, 114, F03016. <https://doi.org/10.1029/2008JF001133>
- Vargas-Luna, A., Crosato, A., & Uijtewaal, W. S. J. J. (2015). Effects of vegetation on flow and sediment transport: Comparative analyses and validation of predicting models. *Earth Surface Processes and Landforms*, 40(2), 157–176. <https://doi.org/10.1002/esp.3633>
- Werner, M., Hunter, N., & Bates, P. (2005). Identifiability of distributed floodplain roughness values in flood extent estimation. *Journal of Hydrology*, 314(1–4), 139–157. <https://doi.org/10.1016/j.jhydrol.2005.03.012>
- Whipple, K. X., Dibiase, R. A., & Crosby, B. (2013). Bedrock rivers. In J. Schreder & E. Wohl (Eds.), *Treatise on Geomorphology* (pp. 550–573). San Diego, CA: Academic Press.
- Whipple, K. X., & Tucker, G. E. (1999). Dynamics of the stream-power river incision model: Implications for height limits of mountain ranges, landscape response timescales, and research needs. *Journal of Geophysical Research*, 104(B8), 17661–17674. <https://doi.org/10.1029/1999JB900120>
- Wright, S., & Parker, G. (2003). Grain-size specific suspended sediment transport and flow resistance in large sand-bed rivers. In A. Gyr & W. Kinzelbach (Eds.), *Sedimentation and Sediment Transport* (pp. 221–227). Dordrecht: Springer.
- Williams, G. P. (1978). Bank-full discharge of rivers. *Water Resources Research*, 14(6), 1141–1154. <https://doi.org/10.1029/WR014i006p01141>
- Wolman, M. G., & Miller, J. P. (1960). Magnitude and frequency of forces in geomorphic processes. *The Journal of Geology* <https://doi.org/10.1086/626637>, 68(1), 54–74.
- Yanites, B. J., & Tucker, G. E. (2010). Controls and limits on bedrock channel geometry. *Journal of Geophysical Research*, 115, F04019. <https://doi.org/10.1029/2009JF001601>
- Yanites, B. J., Tucker, G. E., Mueller, K. J., Chen, Y. G., Wilcox, T., Huang, S. Y., & Shi, K. W. (2010). Incision and channel morphology across active structures along the Peikang River, Central Taiwan: Implications for the importance of channel width. *Bulletin of the Geological Society of America*, 122(7–8), 1192–1208. <https://doi.org/10.1130/B30035.1>